NRC Research Press

ARTICLE

New models for heat flux splitting at the boundary of a porous medium: three energy equations for nanofluid flow under local thermal nonequilibrium conditions

M. Nazari, M.J. Maghrebi, T. Armaghani, and Ali J. Chamkha

Abstract: One of the challenging points in the simulation of a nanofluid flowing through a porous medium is modeling the surface heat flux in the presence of nanoparticles and internal solid matrix. The question is how much energy is absorbed by the solid phase, fluid phase, and particles at the surface of imposing heat flux? To reach a suitable answer, a local thermal nonequilibrium approach (including three energy equations) is presented in this paper and three heat flux models are proposed for the first time. The proposed models are compared and analyzed. The effects of interstitial heat transfer coefficients on the heat transfer in a porous channel are completely studied. The fluid temperature distributions and heat transfer rate obtained by homogenous and nonhomogenous approaches (for the proposed models) are completely studied and compared. The results show that the nonhomogeneous approach experiences larger Nusselt number than the homogeneous one for all the recommended heat flux models.

PACS Nos.: 47.61.–k, 47.56.+r.

Résumé : Une des difficultés dans la simulation de l'écoulement d'un nanofluide à travers un milieu poreux est la modélisation de l'échange de chaleur à la surface en présence de nanoparticules et d'une matrice solide. La question est, combien de chaleur est absorbée par la phase solide, la phase fluide et les particules à la surface où on retrouve le flux de chaleur. Afin de répondre à cette question, nous présentons ici pour la première fois une approche de non équilibre thermique local (incluant les équations d'énergie libre) et proposons trois modèles de flux de chaleur. Les modèles proposés sont comparés et analysés. Nous faisons une étude complète des effets des coefficients de transfert interstitiel de chaleur sur le transfert de chaleur dans un canal poreux. Nous complétons une étude comparative des distributions de température du fluide et de transfert de chaleur obtenues par approches homogène et non homogène (pour nos modèles). Les résultats montrent que l'approche non homogène produit des valeurs plus élevées du nombre de Nusselt, et ce pour tous les modèles présentés de flux de chaleur. [Traduit par la Rédaction]

Introduction

Convective flow and heat transfer in porous media has received considerable attention because of its applications, such as heat pipe, solid matrix heat exchangers, electronic cooling, and drying processes [1]. Local thermal equilibrium (LTE) and local thermal non-equilibrium (LTNE) models are two assumptions for analysis of heat transfer in porous media. Although the LTE model is more convenient to use, more studies have reported that the LTE model is not valid for some problems, such as storage of thermal energy or heat transfer in porous media with internal heat generation. In the case of LTNE, at any chosen point the average fluid temperature is not necessarily the same as the average solid temperature. A suitable example of LTNE is the sudden influx of a cold fluid into a hot porous medium: the mean solid temperature is high initially while the fluid average is cold. Eventually, these temperatures will tend towards an equilibrium where they are the same. In the LTNE model, two energy equations are written for solid and fluid phases. Each energy equation (one for the fluid phase and the other for the solid phase) requires a boundary condition at the solid and fluid boundaries. Many researchers have devoted considerable attention to this subject. Amiri et al. [2] was one of the first to attempt to highlight this problem and present two different approaches of boundary conditions for constant wall heat flux. Martin et al. [3] used the first approach with the assumption of LTE at the wall. Jian and Ren [4] considered four boundary conditions for the case of constant wall heat flux. The proposed boundary conditions were composed of the two approaches introduced by Amiri et al. [2], and the model presented by Martin [3]. Alazmi and Vafai [5] also studied and investigated the effects of using different boundary conditions and they presented five pertinent boundary conditions.

Although convective flow in a duct filled with a porous medium is a promising method of heat transfer enhancement, it is well known that conventional heat transfer pure fluids have poor heat transfer performances because of their heat transfer coefficients between the heat transfer medium and the heat transfer surface. An innovative technique for improving heat transfer by using ultrafine solid particles in the fluids has been widely used recently. Nanofluids, a name conceived by Choi [6] at Argonne National Laboratory, are fluids consisting of solid nanoparticles with size less than 100 nm suspended with solid volume fraction typically less than 4%. Nanofluids can enhance heat transfer performance compared to pure liquids and can be used to improve thermal management systems in many engineering applications, such as transportation, micromechanics and instruments, HVAC sys-

Received 2 September 2013. Accepted 16 January 2014.

M. Nazari. Department of Mechanical Engineering, Shahrood University of Technology, Shahrood, Iran.
M.J. Maghrebi. Department of Mechanical Engineering, Ferdowsi University Of Mashhad, Mashhad, Iran.
T. Armaghani. Department of Engineering, Mahdishahr Branch, Islamic Azad University, Mahdishahr, Iran.
A.J. Chamkha. Manufacturing Engineering Department, The Public Authority for Applied Education and Training, Shuweikh 70654, Kuwait.
Corresponding author: T. Armaghani (e-mail: taherarmaghani@yahoo.com).

tems, and cooling devices. Recently, many investigators studied nanofluid convective heat transfer in different geometries, both numerically and experimentally [7–11]. For numerical simulation, two approaches have been adopted in the literature to investigate the heat transfer characteristics of nanofluids: the single phase model and the two-phase model. Another approach is to adopt the Boltzmann theory [12]. In the single phase model, a uniform volume fraction distribution is assumed for nanofluids. In other words, the viscosity and thermal conductivity of nanofluids are formulated by volume fraction and nanoparticle size. Then, continuity, momentum, and energy equations are solved for nanofluids. In the two-phase model, the volume fraction distribution equation is added to the other conservation equations. Many investors used single and two-phase models for investigating the flow and heat transfer of nanofluids [13–15]. Buongiorno [16] introduced seven slip mechanisms between nanoparticles and the base fluid and showed that the Brownian motion (movement of nanoparticles from high concentration site) and thermophoresis (movement of nanoparticles from high temperature site to the low temperature site) are important parameters in the laminar forced convection of nanofluids. Based on this finding, nonhomogeneous two-component equations in nanofluids were developed. Heyhat and Kowsary [17] used Buongiorno's equations to investigate the effect of particle migration on flow and convective heat transfer of nanofluids flowing through a circular pipe. Results show that the nonuniform distribution leads to a higher heat transfer coefficient while the wall shear stress is decreased. Therefore, the particle migration can play an important role in improvement of the heat transfer coefficient in convective heat transfer in nanofluids.

In recent papers [18–20] Buongiorno's model was applied to the Horton–Rogres–Lapwood problem. The authors studied the onset of convention in a horizontal layer of a porous medium uniformly heated from below. Both Brownian motion and thermophoresis give rise to cross-diffusion terms that are in some way analogous to the familiar Sort and Dufour cross-diffusion terms that arise with a binary fluid. These authors [21] also introduced an analytical treatment of double-diffusive natural convection boundary layer flow in a porous medium saturated by nanofluid. They used Buongiorno's equation to model the nanofluid and the Darcy model for porous medium. The results of the authors showed a decrease in the reduced Nusselt number associated with an increase in the thickness of the thermal boundary layer, an increase in the Brownian motion parameter, buoyancy ratio, thermophoresis parameter, modified Dufour parameter, and a decrease in regular buoyancy ratio. The analytical treatment of double-diffusive natural convection boundary layer flow of a nanofluid past a vertical plate was also studied by Kuznetsov and Nield [22].

The effect of LTNE on the onset of convection in a nanofluid and thermal instability in a porous medium layer (saturated by a nanofluid) are investigated by Niled and Kuznetsov [22, 23]. They assumed that no nanoparticle agglomeration occurs and the nanoparticle suspension remains stable. There are experimental techniques that make it possible to prepare nanoparticle suspensions that remain stable for several weeks [24]. They treat the nanofluid as a continuum, using quantities averaged over a representative elementary volume, a procedure common in the study of flow in a saturated porous medium.

The papers related to LTNE models used three energy equations for solid, nanoparticles, and fluid. The effects of particle migration on forced convective heat transfer of nanofluid in a porous channel at the LTE condition are also investigated by Maghrebi et al. [25]. They show that the particle migration has a significant role in heat transfer. The results show that the local Nusselt number is decreased when the Lewis number is increased. It is observed that as the Lewis number is increased, the wall temperature gradient is decreased and as a consequence the local Nusselt number is decreased. The effects of Lewis number, Schmidt number, and modified diffusivity ratio on the volume fraction distribution are also studied and discussed. In the recent paper written by Armaghani et al. [26], the effects of particle migration in a porous channel on nanofluid convective heat transfer are completely studied when the assumption of LTNE is valid between the phases.

Regarding the published papers, one of the main and challenging points in the simulation of nanofluid flowing through porous media is modeling the surface heat flux in the presence of nanoparticles and internal solid matrix. The question is how much energy is absorbed by the solid phase, fluid phase, and the particles at the surface of imposing heat flux?

The LTNE approach is presented in this paper and three heat flux models are proposed for the first time. The proposed models are also compared and analyzed. The effects of nonhomogenous volume fraction models (against homogenous models) on heat transfer rate are analyzed for all the presented models.

Geometry of the problem

The geometry of the present problem is a two-dimensional channel totally occupied with a porous medium as shown in Fig. 1. Cartesian coordinates are used for this geometry. The height of the channel is equal to $2H$.

Mathematical model

The forced convection heat transfer in a two-dimensional channel is investigated by solving numerically the mathematical formulations introduced in this section. The channel is occupied with a saturated porous medium. The nanofluid, which is treated as a two-component mixture, flows in the channel as discussed by Buongiorno [16]. The fully developed and steady Darcy–Brinkman equation can be used for fluid flow in porous medium. The Brinkman term in this equation represents viscous effects and makes it possible to impose a no-slip boundary condition at the impermeable wall.

$$\frac{\mu_f}{\varepsilon}\nabla^2 u - \frac{\mu_f}{K}u - \frac{dP}{dx} = 0 \tag{1}$$

A three-phase model (in porous media) for nanofluid heat transfer under the LTNE condition was introduced by Kuznetsov and Nield [19]. The dimensionless energy equations for fluid, particles, and solid are given as follows, respectively:

$$(\rho c)_f\frac{\partial T_f}{\partial t} + (\rho c)_f u\frac{\partial T_f}{\partial x} = k_f\nabla^2 T_f + \varepsilon(\rho c)_P\left(D_B\nabla\varphi\cdot\nabla T_f + \frac{D_T}{T_C}\nabla T_f\cdot\nabla T_f\right) + h_{fp}(T_P - T_f) + h_{fs}(T_S - T_f) \tag{2}$$

$$\varepsilon\varphi_0(\rho c)_P\left(\frac{\partial T_P}{\partial t} + \frac{1}{\varepsilon}u\cdot\nabla T_P\right) = \varepsilon\varphi_0 k_P\nabla^2 T_P + h_{fp}(T_f - T_P) \tag{3}$$

$$(1-\varepsilon)(\rho c)_s\frac{\partial T_s}{\partial t} = k_s\nabla^2 T_s + h_{fs}(T_f - T_s) \tag{4}$$

It is obvious that there is a heat transfer between solid and fluid phases as well as that between particles and base fluid. The volume fraction distribution is given as follows:

$$\frac{\partial\varphi}{\partial t} + \frac{1}{\varepsilon}u\cdot\nabla\varphi = D_B\nabla^2\varphi + \frac{D_T}{T_C}\nabla^2 T \tag{5}$$

The Brownian motion and thermophoretic parameters are shown on the right-hand side of (2). Nield et al. [27] indicated that the viscous dissipation term was directly proportional to the Brinkman number defined as $\mu U^2 H/k\Delta TK$ with k, ΔT, and K as conductivity, temperature difference, and permeability. This nondimensional

Fig. 1. Geometry of the present problem and system of coordinates.

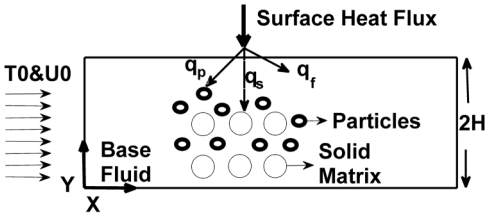

parameter was first defined in (15) of Nield et al. [27]. In the present study the order of magnitude of the aforementioned term is negligible compared with other terms of the energy equation. In other words, as the temperature difference between wall and nanofluid increases, the viscous dissipation can be ignored. This assumption is often made in heat transfer problems in which the temperature (or heat flux) at the surface is the dominant energy source of the system. The dimensionless parameters can be written as

$$u^* = \frac{u}{u_0} \qquad (x^*, y^*) = \frac{(x, y)}{H} \qquad \varphi^* = \frac{\varphi}{\varphi_0} \qquad t^* = \frac{tu_0}{H}$$
$$p^* = \frac{PK}{\mu u_0 H} \qquad \nabla^* = \frac{\partial}{\partial(x^*, y^*)}$$

The dimensionless temperatures for fluid, solid, and nanoparticle are defined as

$$T_f^* = \frac{(T_f - T_0)k_f}{q''H} \qquad T_s^* = \frac{(T_s - T_0)k_s}{q''H} \quad \text{and} \quad T_p^* = \frac{(T_p - T_0)k_p}{q''H}$$

where u_0 is the average velocity in the channel; T_0 and φ_0 are temperature and particle volume fraction at the channel inlet, respectively; T_1 is the wall temperature; and H is characteristic length of the channel.

The dimensionless forms of (1)–(5) can be written as

$$\nabla^{*2}u^* - \frac{u^*}{Da} - \frac{1}{Da}\frac{dP^*}{dx^*} = 0 \tag{6}$$

$$\frac{\partial T_f^*}{\partial t^*} + u^*\frac{\partial T_f^*}{\partial x^*} = \frac{1}{\mathrm{Re\,Pr}}\left[\nabla^{*2}T_f^* + \frac{\tau}{Le}(\nabla^*\varphi^*\cdot\nabla^*T^*) + \frac{\tau}{LeN_{bt}}\left(\nabla^*T_f^*\cdot\nabla^*T_f^*\right) + N_{hp}\left(T_p^* - T_f^*\right) + N_{hs}\left(T_s^* - T_f^*\right)\right] \tag{7}$$

$$\frac{\partial T_p^*}{\partial t^*} + \frac{1}{\varepsilon}u^*\cdot\nabla T_p^* = \frac{1}{\mathrm{Re\,Pr}}\left[\varepsilon_p\nabla^2T_p^* + \gamma_pN_{hp}\left(T_f^* - T_p^*\right)\right] \tag{8}$$

$$\frac{\partial T_s^*}{\partial t^*} = \frac{1}{\mathrm{Re\,Pr}}\left[\varepsilon_s\nabla^2T_s^* + \gamma_sN_{hs}\left(T_f^* - T_s^*\right)\right] \tag{9}$$

It is obvious that under steady state conditions, the Peclet number does not play any role in solid phase temperature. The particle volume fraction equation can be expressed as

$$\frac{\partial \varphi^*}{\partial t^*} + \frac{1}{\varepsilon}u^*\cdot\frac{\partial \varphi^*}{\partial x^*} = \frac{1}{\mathrm{Re\,Sc}}\left[\nabla^2\varphi^* + \frac{1}{N_{bt}}\left(\nabla^2T_f^*\right)\right] \tag{10}$$

The dimensionless parameters are defined as follows:

$$Da = \frac{K}{H^2\varepsilon} \tag{11a}$$

$$N_{bt} = \frac{D_B\varphi_0T_1}{D_T\Delta T} \tag{11b}$$

$$Sc = \frac{\mu}{\rho D_B} \tag{11c}$$

$$Le = \frac{\alpha_f}{D_B\varphi_0} \tag{11d}$$

$$\mathrm{Re} = \frac{u_0H}{\nu} \tag{11e}$$

$$\mathrm{Pr} = \frac{\nu}{\alpha_f} \tag{11f}$$

$$\alpha_f = \frac{k_f}{(\rho c)_f} \tag{11g}$$

$$\tau = \frac{\varepsilon(\rho c)_p}{(\rho c)_f} \tag{11h}$$

$$N_{hp} = \frac{H^2h_{fp}}{\varepsilon(1 - \varphi_0)k_f} \tag{11i}$$

$$N_{hs} = \frac{H^2h_{fs}}{\varepsilon(1 - \varphi_0)k_f} \tag{11j}$$

$$\gamma_p = \frac{(1 - \varphi_0)}{\varphi_0}\frac{(\rho c)_f}{(\rho c)_p} \tag{11k}$$

$$\gamma_s = \frac{\varepsilon(1 - \varphi_0)}{(1 - \varepsilon)}\frac{(\rho c)_f}{(\rho c)_s} \tag{11l}$$

$$\varepsilon_p = \frac{k_p}{k_f}\frac{(\rho c)_f}{(\rho c)_p} \tag{11m}$$

$$\varepsilon_s = \frac{k_s}{k_f}\frac{(\rho c)_f}{(\rho c)_s} \tag{11n}$$

where Da is the Darcy number, Δ is the inertia parameter, Re is the Reynolds number, Sc is the Schmidt number, Pr is the Prantdl number, Le is the nanofluid's Lewis number; τ is modified particle density increment; N_{bt} is a modified diffusivity ratio, which can be expressed as the ratio of Brownian diffusion to the thermophoresis diffusion; γ_p and γ_s are modified thermal capacity ratios; ε_p and ε_s are modified thermal diffusivity ratios; and N_{hp} and N_{hs} are the interface heat transfer parameters. Vadasz [28] called these parameters the Nield numbers, citing Nield [29], and used the parameters in several later papers [30]. In recent literature, the mentioned parameters have been called as the Sparrow numbers. We will follow Vadasz and adopt the terminology of Nield numbers for the fluid–particle interface and fluid–solid-matrix interface.

Boundary and initial conditions

The boundary conditions are as follows:

$$\begin{aligned} &\text{At} \quad y^* = 0, 2 \qquad \varphi^* = 0 \qquad u^* = 0 \\ &\text{At} \quad x^* = 0 \qquad \varphi^* = 1 \end{aligned} \tag{12}$$

For outlet boundary, the normal gradient of properties along the outlet is zero and the values of all properties at the outlet are interpolated from the computational domain.

$$\begin{aligned} &\text{At the channel outlet} \qquad x^* = 20 \qquad \frac{\partial T_f^*}{\partial x^*} = 0 \qquad \frac{\partial T_p^*}{\partial x^*} = 0 \\ &\frac{\partial T_s^*}{\partial x^*} = 0 \qquad \frac{\partial \varphi^*}{\partial x^*} = 0 \end{aligned} \tag{13}$$

The initial conditions, at $t^* = 0$, are

$$T_f^*(t^* = 0) \qquad T_p^*(t^* = 0) \qquad T_s^*(t^* = 0) \quad \text{and} \quad \varphi^*(t^* = 0) = 1 \tag{14}$$

Three proposed models in the presence of nanoparticles in porous media

This paper introduces three thermal models for nanofluid flowing through a porous channel in the case of the LTNE condition. A constant heat flux, q'', is imposed on the impermeable walls of the channel. The incoming heat flux is absorbed by nanoparticles, solid matrix, and base fluid. Following the contributions of each phase from the imposed heat flux, one would have

1. Pure fluid contribution from the imposing heat flux

$$q_f'' = \varepsilon(1 - \varphi)k_f \frac{\partial T_f}{\partial y} \tag{15a}$$

2. Nanoparticle contribution from the boundary heat flux

$$q_f'' = \varepsilon\varphi k_p \frac{\partial T_p}{\partial y} \tag{15b}$$

3. Solid matrix contribution from the total heat flux

$$q_f'' = (1 - \varepsilon)k_s \frac{\partial T_s}{\partial y} \tag{15c}$$

Then, the total heat flux can be written as

$$q'' = q_f'' + q_p'' + q_s'' = \varepsilon(1 - \varphi)k_f\left(\frac{\partial T_f}{\partial y}\right)_{wall} + \varepsilon(\varphi)k_p\left(\frac{\partial T_p}{\partial y}\right)_{wall} + (1 - \varepsilon)k_s\left(\frac{\partial T_s}{\partial y}\right)_{wall} \tag{16}$$

The dimensionless form of (16) is

$$1 = \varepsilon\left(1 - \phi^*\phi_0\right)\left(\frac{\partial T_f^*}{\partial y^*}\right)_{wall} + \varepsilon\left(\phi^*\phi_0\right)\frac{k_p}{k_f}\left(\frac{\partial T_p^*}{\partial y^*}\right)_{wall} + (1 - \varepsilon)\frac{k_s}{k_f}\left(\frac{\partial T_f^*}{\partial y^*}\right)_{wall} \tag{17}$$

Now, we introduce three thermal boundary condition models for nanofluid in a porous channel, heated by constant heat flux

Model 1

In the first model, the heat flux ratio (between the phases) is related to the occupied space of solid matrix, base fluid, and nanoparticles

$$\frac{q_f''}{q_s''} = \frac{\varepsilon(1 - \varphi^*\varphi_0)}{1 - \varepsilon} \qquad \frac{q_f''}{q_p''} = \frac{\varepsilon(1 - \varphi^*\varphi_0)}{\varepsilon\varphi^*\varphi_0} \tag{18}$$

After some manipulation, one can obtain the following relation:

$$\frac{\partial T_f^*}{\partial y^*} = \frac{\partial T_p^*}{\partial y^*} \qquad \frac{\partial T_f^*}{\partial y^*} = \frac{\partial T_s^*}{\partial y^*} \tag{19}$$

Substituting (19) into (17), one can find that

$$\frac{\partial T_f^*}{\partial y^*}\left[\varepsilon(1 - \varphi^*\varphi_0) + (1 - \varepsilon) + \varepsilon\varphi^*\varphi_0\right] = 1 \tag{20}$$

then

$$\frac{\partial T_f^*}{\partial y^*} = 1 \qquad \frac{\partial T_p^*}{\partial y^*} = 1 \quad \text{and} \quad \frac{\partial T_s^*}{\partial y^*} = 1 \tag{21}$$

Model 2

In the second view, the heat flux ratio can be related to the solid, base fluid, and nanoparticles conductivity

$$\frac{q_f''}{q_s''} = \frac{k_f}{k_s} \qquad \frac{q_f''}{q_p''} = \frac{k_f}{k_p} \tag{22}$$

which can be expressed as

$$\frac{\partial T_f^*}{\partial y^*} = \frac{\varepsilon\varphi^*\varphi_0}{\varepsilon(1 - \varphi^*\varphi_0)}\frac{k_f}{k_p}\frac{\partial T_p^*}{\partial y^*} \qquad \frac{\partial T_f^*}{\partial y^*} = \frac{(1 - \varphi^*\varphi_0)}{\varepsilon(1 - \varphi^*\varphi_0)}\frac{k_f}{k_s}\frac{\partial T_s^*}{\partial y^*} \tag{23}$$

Substituting (23) into (17), one can find

$$\frac{\partial T_f^*}{\partial y^*}\left[\varepsilon(1 - \varphi^*\varphi_0) + \varepsilon(1 - \varphi^*\varphi_0)\frac{k_p}{k_f} + \varepsilon(1 - \varphi^*\varphi_0)\frac{k_s}{k_f}\right] = 1 \tag{24}$$

$$\frac{\partial T_f^*}{\partial y^*} = \frac{1}{\varepsilon(1 - \varphi^*\varphi_0)}\frac{k_f}{(k_f + k_p + k_s)} \tag{25a}$$

$$\frac{\partial T_p^*}{\partial y^*} = \frac{1}{\varepsilon\varphi^*\varphi_0}\frac{k_p}{(k_f + k_p + k_s)} \tag{25b}$$

$$\frac{\partial T_s^*}{\partial y^*} = \frac{1}{(1 - \varepsilon)}\frac{k_s}{(k_f + k_p + k_s)} \tag{25c}$$

Model 3

The third model is a combination of models 1 and 2. It includes the effects of porosity, volume fraction, and conductivity as follows:

$$\frac{q_f''}{q_s''} = \frac{k_f}{k_s}\frac{\varepsilon(1 - \varphi^*\varphi_0)}{1 - \varepsilon} \qquad \frac{q_f''}{q_p''} = \frac{k_f}{k_p}\frac{\varepsilon(1 - \varphi^*\varphi_0)}{\varepsilon\varphi^*\varphi_0} \tag{26}$$

and after some mathematical manipulation, one can find that

$$\frac{\partial T_f^*}{\partial y^*} = \frac{k_f}{k_p}\frac{\partial T_p^*}{\partial y^*} \qquad \frac{\partial T_f^*}{\partial y^*} = \frac{k_f}{k_s}\frac{\partial T_s^*}{\partial y^*} \tag{27}$$

Substituting (27) into (17)

$$\frac{\partial T_f^*}{\partial y^*}\left[\varepsilon(1-\varphi^*\varphi_0) + \varepsilon\varphi^*\varphi_0\frac{k_p}{k_f} + (1-\varepsilon)\frac{k_s}{k_f}\right] = 1 \tag{28}$$

$$\frac{\partial T_f^*}{\partial y^*} = \frac{k_f}{\varepsilon(1-\varphi^*\varphi_0)k_f + \varepsilon\varphi^*\varphi_0 k_p + (1-\varepsilon)k_s} \tag{29a}$$

$$\frac{\partial T_s^*}{\partial y^*} = \frac{k_s}{\varepsilon(1-\varphi^*\varphi_0)k_f + \varepsilon\varphi^*\varphi_0 k_p + (1-\varepsilon)k_s} \tag{29b}$$

$$\frac{\partial T_p^*}{\partial y^*} = \frac{k_p}{\varepsilon(1-\varphi^*\varphi_0)k_f + \varepsilon\varphi^*\varphi_0 k_p + (1-\varepsilon)k_s} \tag{29c}$$

Finally, we introduced three Nusselt numbers for fluid, nanoparticles, and solid matrix. Amiri and Vafai [31] introduced both fluid and solid Nusselt numbers for LTNE porous medium. This paper presents fluid, nanoparticle, and solid matrix Nusselt numbers for nanofluid flowing through LTNE porous channel as follows:

$$\mathrm{Nu}_f = -\frac{2}{(T_f^*)_W - T_{mf}^*}\left(\frac{\partial T_f^*}{\partial y^*}\right)_{wall} \qquad T_{mf}^* = \frac{\int_0^2 u^* T_f^* dy^*}{U_m^*} \tag{30}$$

$$\mathrm{Nu}_p = -\frac{2}{(T_p^*)_W - T_{mp}^*}\left(\frac{\partial T_p^*}{\partial y^*}\right)_{wall} \qquad T_{mp}^* = \frac{\int_0^2 u^* T_p^* dy^*}{U_m^*} \tag{31}$$

The mean velocity in (30) and (31) is the nanofluid mean velocity, which can be defined as

$$U_m^* = \int_0^2 u^* dy^* \qquad \mathrm{Nu}_s = -\frac{2}{(T_s^*)_W - T_{ms}^*}\left(\frac{\partial T_s^*}{\partial y^*}\right)_{wall} \qquad T_{ms}^* = \int_0^2 T_s^* dy^* \tag{32}$$

Numerical strategy and computational procedure

The finite difference method is used to solve the governing equations, (6)–(10). The fully implicit method is employed to discretize the time-dependant terms. It is interesting to notice that the thermophoretic parameter, ∇T^*, is linearized by the method specified in Patankar [32]. The uniform grids are used in the computational domain. The results of grid independency are given in Table 1. In our previous research work [25], the nonlinear Darcy–Brinkmann–Forchheimer equation is solved using the Newton–Raphson method [33]. For simplicity, the Darcy–Brinkmann equation is used in this study. The coupled energy and volume fraction distribution equations are solved using a line-by-line iterative procedure that sweeps the computational domain in the x–y direction. The computational procedure for the solution of governing equations can be summarized as follows:

1. Solve the Darcy–Brinkman equation to obtain the axial velocity (u).
2. Use the obtained velocity and solve the fluid temperature equation to recover T_f.
3. Use the obtained T_f and solve the particle temperature equation to recover T_p.
4. Use the obtained T_f and solve the particle temperature equation to recover T_s.
5. Use the new values of T_f in the volume fraction distribution equation to obtain the new φ.
6. Calculate the absolute error, if $|T_f^{n+1} - T_f^n| > 10^{-15}$ and $|T_s^{n+1} - T_s^n| > 10^{-15}$. If $|T_p^{n+1} - T_p^n| > 10^{-15}$ and $|\varphi^{n+1} - \varphi^n| > 10^{-15}$ return to step 2 using new φ, T_s, and T_p.

Table 1. Grid study.

Number of grids	Fully developed Nusselt number
100×100	8.234
200×200	8.234
300×300	8.235
400×400	8.235

Results

Validation

The present problem can be transformed into a simple channel-flow problem as the porosity approaches one. In this case the local Nusselt number is calculated and compared with the results of Shah and London [34] and that of Bejan [35]. As shown in Fig. 2, the fully developed Nusselt number in the channel with constant wall heat flux is 8.23. The fully developed velocity distribution in the porous channel can be obtained analytically as $\Delta \to 0$. Moreover, for checking the accuracy of numerical solution of (8) and (9), the fluid temperature distribution in the case of thermal equilibrium is derived from our previous published paper and inserted into the present code (with constant wall temperature boundary condition). Then, we set $N_{hs} = 10^6$ and $N_{hp} = 10^6$ in the simulation. As shown in Fig. 3, both solid temperature and particle temperature distributions fully overlap the fluid temperature distribution. As expected, large values of N_{hs} and N_{hp} correspond to thermal equilibrium condition.

Discussion about the proposed models

In the present paper, the following parameters are selected for the numerical simulation: $\varphi_0 = 0.05$, $\gamma_p = 10$, $\gamma_s = 10$, $Pr = 1$, $Re = 150$, $\tau = 1$, $\varepsilon_s = 500$, $\varepsilon_p = 100$, $[1/(DaH^2)](dP^*/dx^*) = -2$. The thermal conductivities are also fixed at $k_p = 50$, $k_s = 250$, and $k_f = 0.5$, which are values for alumina, aluminum, and water, respectively.

Figure 4 shows the dimensionless fluid temperature distribution for the three proposed thermal models. As shown in the figure, two different values are selected for N_{hp}: 1 and 100. Figure 4*a* shows that the fluid dimensionless temperature varies by changing N_{hp} and a significant variation of temperature is observed in model 1. In other words, increasing the value of N_{hp} results in a visible change in the fluid temperature predicted by model 1. Figure 4*b* also shows a closer view of models 2 and 3. As shown in this frame, increasing the value of N_{hp} leads to an increase in the fluid temperature in the wall vicinity. This trend is not observed in model 1, which is mainly because of effects of thermal conductivity of the phases appearing in models 2 and 3. Strictly speaking, one can refer to (29); by neglecting the thermal conductivity of the phases (i.e., k_s, k_p, and k_f) in the preceding equation, model 1 is recovered. When N_{hp} is increased, the fluid

Fig. 2. Comparison of local Nusselt number in the present work and the analytical solution, as $\varepsilon \to 1$.

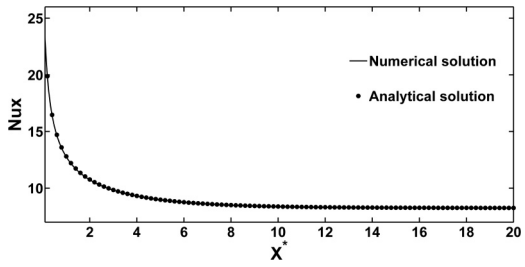

Fig. 3. Fluid, solid, and particle temperatures at $N_{hs} = 10^6$ and $N_{hp} = 10^6$.

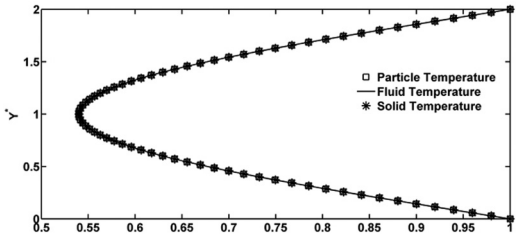

Fig. 4. (*a*) Dimensionless fluid temperature obtained by the proposed models for different values of N_{hp}, $N_{hs} = 1$, (*b*) a closer view.

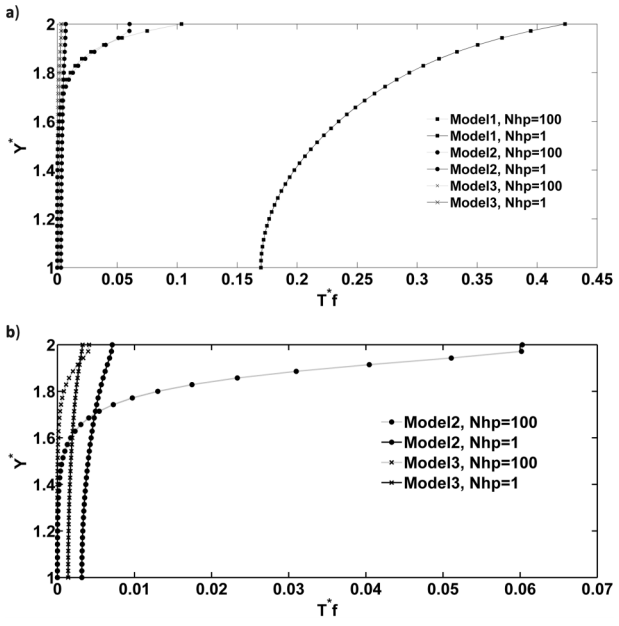

Fig. 5. Dimensionless fluid temperature obtained by models 2 and 3 for different values of N_{hs} at $N_{hp} = 1$.

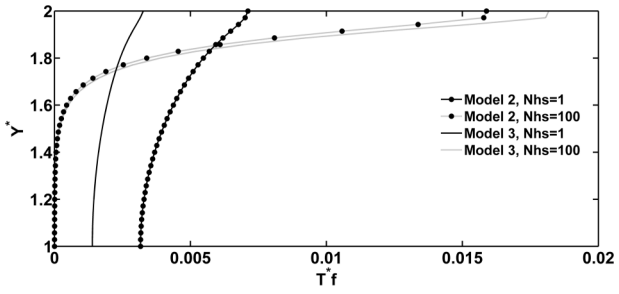

Fig. 6. Dimensionless nanoparticle temperature obtained by the proposed models at $N_{hp} = N_{hs} = 1$.

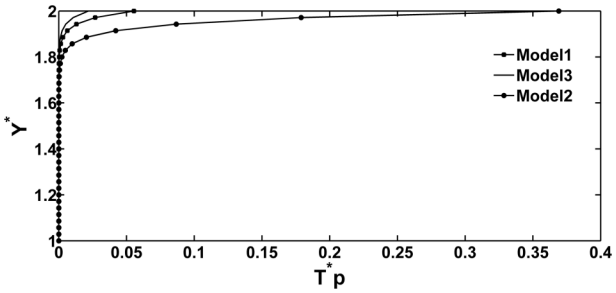

Fig. 7. Dimensionless fluid temperature obtained by the presented models at $N_{hp} = N_{hs} = 1$.

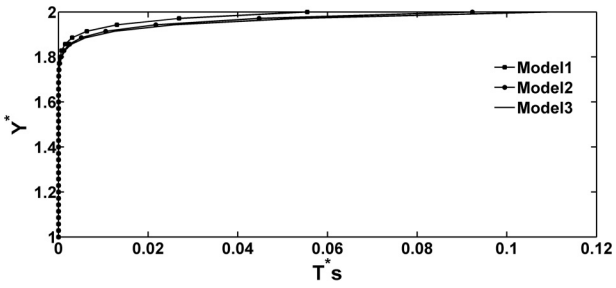

Fig. 8. Comparison of fluid temperature between homogenous and nonhomogenous approaches, (*a*) results of model 1, (*b*) results of models 2 and 3.

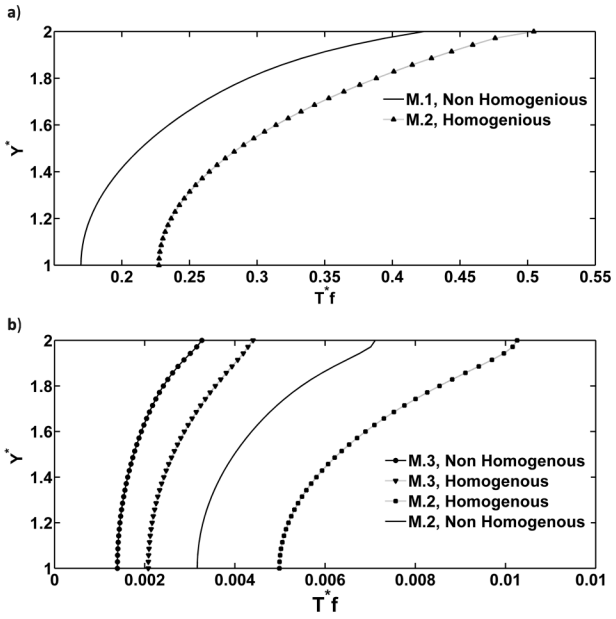

dimensionless temperature is increased in the region near the wall and it decreases at the center of the channel. One can find that N_{hp} is the important parameter in the fluid energy equation.

Figure 5 shows the effects of N_{hs} on the fluid dimensionless temperature for two models. The general trend in this figure is similar to Fig. 4. As discussed before, the temperature data obtained by model 1 is different from that obtained by other models that reflect the effects of thermal conductivity ratios.

Table 2. The Nusselt number of the fluid phase (Nu_f) obtained by the three proposed models for $N_{hp} = 1$ and $N_{hs} = 1$.

	Nonhomogenous model	Homogenous model
M.1	10.28	9.91
M.2	2.45	1.93
M.3	5.68	4.85

Fig. 9. Various fully developed Nusselt number with different N_{hp}: (*a*) fully developed fluid Nusselt number, (*b*) fully developed particle Nusselt number, and (*c*) fully developed solid Nusselt number.

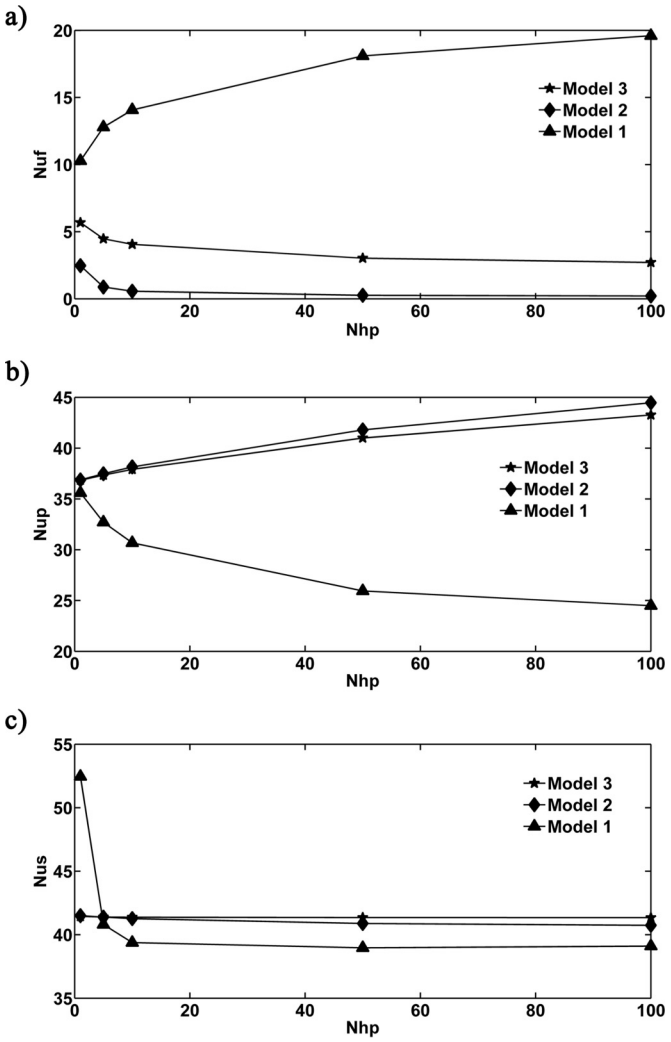

Figure 6 shows the particle temperature distribution for the three models when $N_{hs} = 1$. The obtained results show that particle dimensionless temperatures (for all the mentioned models) do not experience any significant change by increasing N_{hs}. As presented in this figure, the maximum temperature near the wall is related to model 2, and the minimum values of the temperature are obtained by model 3.

Figure 7 shows the trend of the solid dimensionless temperature by variation of N_{hs}. The results confirm that changing the values of N_{hs} (and also N_{hp}) have no major effect on the solid dimensionless temperature, for all the mentioned models.

Fig. 10. Various fully developed Nusselt number with different N_{hs}: (*a*) fully developed fluid Nusselt number, (*b*) fully developed particles Nusselt number, and (*c*) fully developed solid Nusselt number.

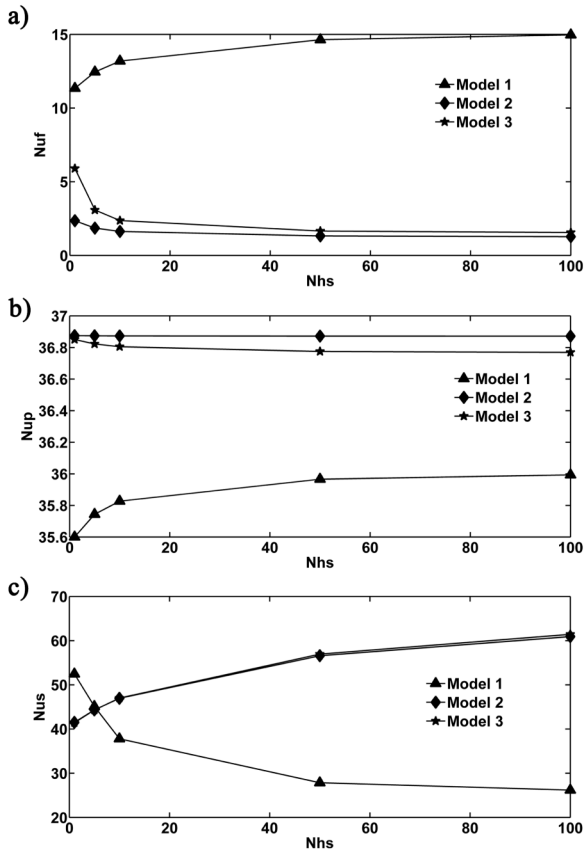

Figure 8 shows the fluid temperature in the channel for both cases of homogenous and nonhomogenous approaches. The nonhomogenous approach is obtained by solving the momentum equation, three energy equations and mass conversion of nanoparticles. Another approach is obtained by solving momentum and three energy equations without particle distribution effects. In other words, the initial volume fraction of nanoparticles is kept constant in the entire computational domain in the case of the homogenous approach. In this figure, we use $N_{hp} = N_{hs} = 1$. The comparison between the two approaches shows that the fluid temperature in the case of the homogeneous approach is larger than that of the nonhomogenous approach. The difference between these two approaches can be related to the effects of volume fraction of nanoparticles in the porous channel.

The local Nusselt number at the thermally fully developed region of the channel is presented in Table 2 for both nonhomogenous and homogenous approaches. One can find from this table that the Nusselt number predicted by model 1 has maximum value.

Figure 9 shows the fully developed Nusselt number for different values of N_{hp}. As shown Fig. 9*a*, the fully-developed fluid Nusselt number (obtained by model 1) increases by increasing N_{hp}; but in the models 2 and 3, a decreasing trend is observed. The fully developed solid-phase Nusselt number is shown in Fig. 9*b*. The solid-phase Nusselt number decreases by increasing N_{hp} in model 1. The variations of solid-phase Nusselt number with N_{hp} are not significant in models 2 and 3. In model 1, the fully developed particle-phase Nusselt number decreases when N_{hp} increases (see Fig. 9*c*).

Figure 10 shows the fully developed Nusselt number by changing N_{hs}. The trend of variations of Nusselt number in this figure is similar to Fig. 9.

Which model is suitable for simulation of nanofluid in a porous medium?

The results show that the Nusselt numbers (for fluid, solid, and particles phases) predicted by model 1 are maximized. For all the proposed models, the nonhomogeneous approach experiences larger Nusselt number than the homogeneous view. The trend of variations of the results of models 2 and 3 are similar. Therefore, we propose these two models for simulation of nanofluid flow in porous media. Nonetheless, an experimental setup can be designed to verify this conclusion.

Conclusion

This paper was concerned with nanofluid flow and heat transfer in a straight channel occupied with a porous medium. The fully-developed flow and steady Darcy–Brinkman equation was employed in the porous channel. It was assumed that the nanoparticles are distributed nonuniformly inside the channel. The LTNE approach (including three energy equations) is presented in this paper. Three heat flux models are proposed for the first time. The proposed models are also compared and analyzed. The results show that the Nusselt numbers (for fluid, solid, and particle phases) predicted by model 1 are maximized. For all the proposed models, the nonhomogeneous approach experiences larger Nusselt number than the homogeneous view. The trend of variations of the results of models 2 and 3 are similar. Therefore, we propose these two models for simulation of nanofluid flow in porous media. Nonetheless, an experimental setup can be designed to verify this conclusion. In the future, we will also examine the nanofluid flow experimentally to validate the proposed models of this paper.

References

1. K. Yang and K. Vafai. J. Heat Transfer, **133**, 052602-1-11 (2011).
2. A. Amiri, K. Vafai, and T.M. Kuzay. Numer. Heat Transfer, Part A, **27**, 651 (1995). doi:10.1080/10407789508913724.
3. A.R. Martin, C. Saltiel, and W. Shy. J. Heat Transfer, **120**, 458 (1998). doi:10.1115/1.2824271.
4. P.X. Jiang and Z.P. Ren. Int. J. Heat Fluid Flow, **22**, 102 (2001). doi:10.1016/S0142-727X(00)00066-7.
5. B. Alazmi and K. Vafai. Int. J. Heat Mass Transfer, **45**, 3071 (2002). doi:10.1016/S0017-9310(02)00044-3.
6. S.U.S. Choi. Dev. Appl. Non-Newtonian Flows, **66**, 99 (1995).
7. S.E.B. Maiga, C.T. Nguyen, N. Galanis, and G. Roy. Superlattices Microstruct. **35**, 453 (2004).
8. W. Duangthongsuk and S. Wongwises. Int. J. Heat Mass Transfer, **52**, 2059 (2009). doi:10.1016/j.ijheatmasstransfer.2008.10.023.
9. A.K. Santra, S. Sen, and M. Chakraborty. Int. J. Therm. Sci. **48**, 391 (2009). doi:10.1016/j.ijthermalsci.2008.10.004.
10. C.T. Nguyen, N. Galanis, G. Polidori, S. Fohanno, C.V. Popa, and A.L. Bechec. Int. J. Therm. Sci. **48**, 401 (2009). doi:10.1016/j.ijthermalsci.2008.10.007.
11. M.H. Kayhani, H. Soltanzadeh, M.M. Heyhat, M. Nazari, and F. Kowsary. Int. Comm. Heat Mass Transfer, **39**, 456 (2012). doi:10.1016/j.icheatmasstransfer.2012.01.004.
12. X.Q. Wang and A.S. Mujumdar. Int. J. Therm. Sci. **46**, 1 (2007). doi:10.1016/j.ijthermalsci.2006.06.010.
13. A. Behzadmehr, M. Saffar-Avval, and N. Galanis. Int. J. Heat Fluid Flow, **28**, 211 (2007). doi:10.1016/j.ijheatfluidflow.2006.04.006.
14. M.J. Maghrebi, T. Armaghani, and F. Talebi. Therm. Sci. **16**, 455 (2012). doi:10.2298/TSCI101011022M.
15. J. Lee and I. Mudawar. Int. J. Heat Mass Transfer, **50**, 452 (2007). doi:10.1016/j.ijheatmasstransfer.2006.08.001.
16. J. Buongiorno. ASME J. Heat Transfer, **128**, 240 (2006). doi:10.1115/1.2150834.
17. M.M. Heyhat and F. Kowsary. ASME J. Heat Transfer, **132**, 062401 (2010). doi:10.1115/1.4000743.
18. A.V. Kuznetsov and D.A. Nield. Trans. Porous Media, **81**, 409 (2010). doi:10.1007/s11242-009-9413-2.
19. A.V. Kuznetsov and D.A. Nield. Trans. Porous Media, **83**, 425 (2010). doi:10.1007/s11242-009-9452-8.
20. A.V. Kuznetsov and D.A. Nield. J. Porous Media, **14**, 285 (2011). doi:10.1615/JPorMedia.v14.i4.10.
21. A.V. Kuznetsov and D.A. Nield. Int. J. Therm. Sci. **50**, 712 (2011). doi:10.1016/j.ijthermalsci.2011.01.003.
22. D.A. Nield and A.V. Kuznetsov. Int. J. Heat Mass Transfer, **52**, 5796 (2009). doi:10.1016/j.ijheatmasstransfer.2009.07.023.
23. D.A. Nield and A.V. Kuznetsov. ASME J. Heat Transfer, **132**, 052405 (2010). doi:10.1115/1.4000474.
24. K.B. Anoop, T. Sundararajan, and K. Das Sarit. Int. J. Heat Mass Transfer, **52**, 2189 (2009). doi:10.1016/j.ijheatmasstransfer.2007.11.063.
25. M.J. Maghrebi, M. Nazari, and T. Armaghani. Transp. Porous Media, **93**, 401 (2012). doi:10.1007/s11242-012-9959-2.
26. T. Armaghani, M.J. Maghrebi, A.J. Chamkha, and M. Nazari. J. Nanofluids, **3**, 1 (2014). doi:10.1166/jon.2014.1076.
27. D.A. Nield, A.V. Kuznetsov, and M. Xiong. Int. J. Heat Mass Transfer, **46**, 643 (2003). doi:10.1016/S0017-9310(02)00327-7.
28. P. Vadasz. ASME J. Heat Transfer, **128**, 465 (2006). doi:10.1115/1.2175149.
29. D.A. Niled. J. Porous Media, **1**, 181 (1998).
30. P. Vadasz. J. Porous Media, **15**, 249 (2012). doi:10.1615/JPorMedia.v15.i3.40.
31. A. Amiri, K. Vafai, and T.M. Kuzay. Numer. Heat Transfer, Part A, **27**, 651 (1995). doi:10.1080/10407789508913724.
32. S.V. Patankar. Numerical Heat Transfer and Fluid Flow. Hemisphere, New York. 1980.
33. J.F. Epperson. An introduction to numerical methods and analysis. John Wiley & Sons. 2010.
34. R.K. Shah and A.L. London. Laminar Flow Forced Convection in Ducts, supplemental to advances heat transfer. Academic, New York. 1978.
35. A. Bejan. Convective heat transfer, 3rd ed. John Wiley & Sons, Hoboken. 2003.

List of symbols

Da	Darcy number
D_B	Brownian diffusion coefficient (m^2s^{-1})
D_T	Thermophoretic diffusion coefficient (m^2s^{-1})
h_{fp}	Heat transfer coefficient between the fluid–particle
h_{fs}	Heat transfer coefficient between the fluid–solid
H	Half length of channel
k	Thermal conductivity ($wm^{-1}K^{-1}$)
K	Permeability (m^2)
Le	Lewis number
N_{bt}	Brownian motion parameter
N_{hp}	Nield number for the fluid–particle interface
N_{hs}	Nield number for the fluid–solid matrix interface
P	Pressure (Nm^{-2})
Pr	Prandtl number
Re	Reynolds number
Sc	Schmit number
t	Time(s)
T	Temperature (K)
u	Axial velocity (ms^{-1})
x, y	Cartesian coordinate (m)
α	thermal diffusivity (m^2s^{-1})
γ_p	Modified particle thermal capacity ratio by (11*k*)
γ_s	Modified solid thermal capacity ratio by (11*l*)
ε	Porosity
ε_p	Modified particle thermal diffusivity ratio by (11*m*)
ε_s	Modified solid thermal diffusivity ratio by (11*n*).
μ	Viscosity ($kg\ m^{-1}s^{-1}$)
ρ	Density ($kg\ m^{-3}$)
φ	Volume fraction
τ	Modified diffusivity ratio